Journal Name

ARTICLE TYPE

Cite this: DOI: 00.0000/xxxxxxxxxx

Theoretical Investigation of Amino-Acid Adsorption on Hydroxylated Quartz Surfaces: Dispersion can Determine Enantioselectivity

Alastair J. Price[a] and Erin R. Johnson[a,*]

Received Date
Accepted Date

DOI: 00.0000/xxxxxxxxxx

Chiral mineral surfaces, such as quartz, are attractive substrates for use in enantioselective separation and may have contributed to the origin of biological homochirality. In this work, we apply density-functional theory and the exchange-hole dipole moment (XDM) dispersion model to study the adsorption of 5 amino acids (glycine, serine, alanine, valine, and phenylalanine) on a hydroxylated α-quartz (0001) surface. It is demonstrated that London dispersion is responsible for 30–50% of the total adsorption energies and its inclusion or omission can reverse predictions of enantioselectivity. Differing dispersion stabilization, caused by the opposing side-chain placements relative to the quartz surface, lead to differences of 1.0 and 1.8 kcal/mol in the adsorption energies of the alanine and phenylalanine enantiomers, respectively. These results are consistent with a 3-point model, with the hydrogen-bonding sites conserved and variations in the dispersion interactions determining enantioselectivity.

1 Introduction

Molecular chirality is ubiquitous in living systems, making enantioselective synthesis an important step in the development of new pharmaceuticals and other fine chemicals. As many chiral compounds are only found in, or made as, racemic mixtures, development of practical methods for enantiospecific separation remains an ongoing challenge in chemistry. One promising approach to chiral separation is absorption on a chiral substrate,[1–5] which can include chiral nanoparticles[6] or microspheres,[7,8] self-assembled monolayers of amino acids,[9–11] and chiral metal surfaces.[12–17] However, such substrates can be arduous to prepare and may not be thermally stable.

Chiral mineral surfaces, such as quartz, are attractive alternatives for use in enantioselective synthesis[18] and separation[1,2,19] because they are stable, naturally occurring, and unreactive with organic adsorbates. Moreover, quartz surfaces have been shown to enhance homochirality in oligopeptides[20] and have been implicated as a possible origin of homochirality in biology.[21–23] Of particular note, quartz has been demonstrated to have a slight chiral preference for one enantiomer of alanine over the other,[24,25] and the selectivity is increased for alanine derivatives.[19]

Enantiospecific adsorption can be understood through an intuitive 3-point model,[26–29] in which three of the four functional groups about a tetrahedral chiral center can interact directly with the surface. The two strongest intermolecular interactions between the molecule and surface will be conserved between enantiomers, while the nature of the third interaction will vary depending on which of the remaining two functional groups is pointing down to interact with the surface, and which is pointing up, away from it. For adsorption of neutral amino acids, the NH_2 and COOH groups are capable of strong hydrogen bonding with quartz and will likely remain tethered to the surface. Thus, any enantioselectivity will be driven by the differing interaction strengths for the other two substituents of the α carbon, namely the hydrogen atom and amino-acid side chain. This is shown pictorially for alanine in Figure 1. Here, any enantioselectivity will be due to differences in London dispersion interactions between the H and CH_3 substituents with the surface. Given that dispersion is responsible for the 0.5 kcal/mol binding energy of the methane dimer and the 1.4 kcal/mol binding energy of the methane-benzene complex,[30] it is reasonable to expect some enantioselectivity for alanine adsorption on a chiral surface.

Computational modeling of amino acid adsorption on quartz is extremely complex as the experimental system involves adsorption of zwitterions from solution on several possible crystal faces. Such simulations are possible with classical molecular dynamics,[31] but resolving the minute adsorption-energy differences between enantiomers requires more sophisticated methods.[32,33] Quantum-mechanical studies using density-functional theory (DFT) are limited to adsorption of neutral amino acids,

[a] Department of Chemistry, Dalhousie University, 6274 Coburg Road, PO Box 15000 Halifax, Nova Scotia, Canada B3H 4R2. E-mail: erin.johnson@dal.ca

Fig. 1 Representative illustration of the adsorbed configurations for the alanine S and R enantiomers on a surface.

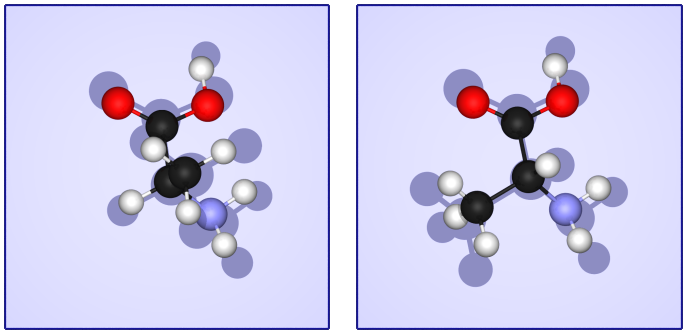

(a) S alanine **(b)** R alanine

Fig. 2 The two possible chiralities for the unit cell of α-quartz: (a) laevorotatory, in the $P3_121$ space group and (b) dextrorotatory in the $P3_221$ space group. Also shown is a top view of the hydroxylated quartz surface used in our computational studies (c). Only the top layers of Si, O, and H atoms at the surface are shown in stick representation for clarity; lower surface layers are shown as SiO_4 tetrahedra. Yellow lines indicate hydrogen bonding.

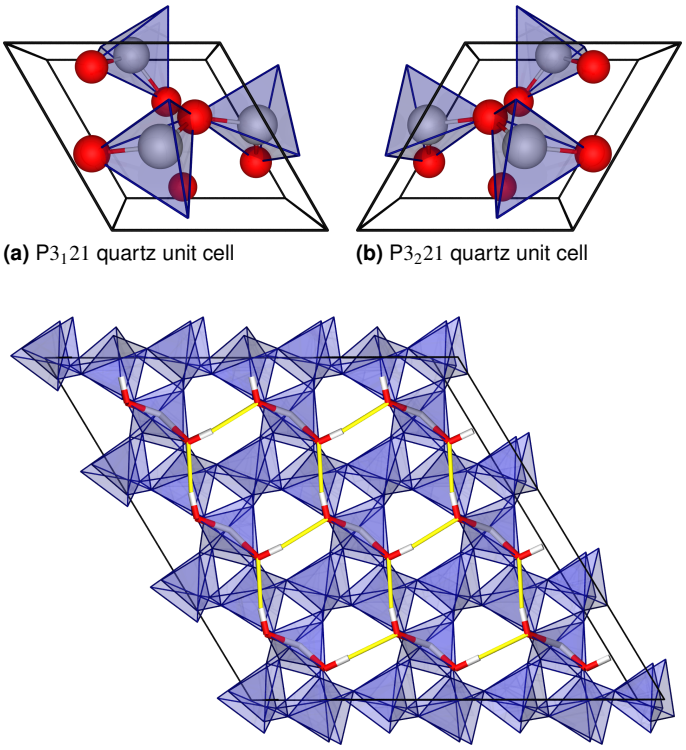

(a) $P3_121$ quartz unit cell **(b)** $P3_221$ quartz unit cell

(c) The model hydroxylated quartz (0001) surface

as the zwitterions are unstable without a surrounding network of hydrogen bonds. Previous DFT studies have considered adsorption of the glycine, alanine, serine, cysteine, aspartic acid, and arginine amino acids on the (0001) and $(10\bar{1}0)$ faces of quartz.[34,35] However, these works showed effectively no chiral preference for alanine, which is counter to what would be expected from the 3-point interaction picture.

The issue with the previous theoretical treatment[34,35] is likely the level of theory, as those works used the PW91 functional,[36] which overestimates H-bond strengths and does not include London dispersion physics.[37–39] We expect that inclusion of dispersion will be necessary to account for the slight differences in adsorption energies between the two enantiomers arising from the subtle variations in their interactions with the surface. However, dispersion is not captured by standard generalised gradient approximation (GGA), meta-GGA, or hybrid functionals[39] since it is a highly non-local correlation effect. Instead, standard functionals must be supplemented with a dispersion-energy term through explicitly non-local correlation functionals[40,41] or through an asymptotic perturbation-theory expansion.[42–45]

The aim of this work is to apply dispersion-corrected DFT to compute the adsorption energies of various amino acids on the α-quartz (0001) surface, and to determine whether there is a chiral preference. In particular, we will use the exchange-hole dipole moment (XDM) dispersion method,[45,46] since it has been shown to provide simultaneous high accuracy for molecular[47,48] and solid-state systems,[47,49,50] as well as for surface adsorption on metals.[51–53] Importantly, XDM is capable of reproducing the small energy differences between homochiral and heterochiral crystal forms of amino acids and other chiral organic molecules.[32,33,54] We consider glycine, alanine, and serine, following the work of Han and Sholl,[34] as well as valine and phenylalanine, due to the significant dispersion interactions expected occur between the hydrophobic side chains and the surface. It is demonstrated that such dispersion interactions surface can give rise to a significant energetic bias for preferential binding of one enantiomer of alanine and phenylalanine.

2 Computational Methods

α-Quartz is the most stable polymorph of silica at ambient conditions and consists of a network of connected SiO_4 tetrahedra. Its chirality is apparent by comparing the two unit cells shown in Figure 2(a,b), which are non-superimposable mirror images. The (0001) hydroxylated quartz surface can be constructed by cleaving the Si-O bonds of α-quartz and terminating the resulting surface (top and bottom) with OH groups. Our model surface, shown in Figure 2(c), corresponds to left-handed quartz, in the $P3_121$ space group.[55] It was generated following the work of Goumans et al.[55] and contains 6 layers of SiO_4 tetrahedra to provide a reasonable treatment of the bulk. The periodic surface was generated with 40 Å of vacuum inserted in the z-dimension between each slab, with the atomic positions and x,y-cell parameters optimised. The resulting structure was then used as the basis for all following calculations with the adsorbed amino acids.

Five amino acids were selected for the adsorption calculations: glycine, serine, alanine, valine, and phenylalanine. Only the neutral forms of the amino acids and not the zwitterions were considered, as the latter are unstable without the influence of neighbouring amino acids or solvent and will revert to the neutral forms on geometry optimisation. The unit cell of the quartz surface was replicated in the x and y directions to generate the

2×2 supercell shown in Figure 2(c). This supercell was used in the adsorption calculations to minimise interactions between the adsorbed amino acid and its periodic images. The positions of all atoms were allowed to relax, but the cell parameters kept fixed at the optimised values for the clean surface. Additional calculations were performed for all possible conformations of the isolated amino acids, in a supercell of the same dimensions as used in the surface calculations, in order to compute the adsorption energies.

The initial geometries of the adsorbed amino acids employed in the calculations were informed by the work of Han and Scholl.[34] For glycine, the two near-degenerate, hydrogen-bonded structures previously reported were built and optimised. For all other amino acids, the main-chain COOH and NH_2 groups were fixed to the same two surface binding sites as for glycine, and structures were generated for all reasonable conformations of the side-chain functional groups. The one exception is serine, in which the positions of both the NH_2 group and the side chain were varied, in order to consider low-energy configurations involving H-bonding between the side-chain OH and the surface.

All DFT calculations were performed with version 5.1 of the Quantum ESPRESSO electronic structure code,[56] planewave basis sets, and pseudopotentials, using the projector augmented-wave (PAW) framework.[57] The B86bPBE exchange-correlation functional[58,59] and the XDM dispersion correction were used throughout.[45–47] The XDM a_1 and a_2 damping parameters were set to their canonical values of 0.6512 and 1.4633 Å, respectively. Tight convergence criteria of 10^{-5} and 10^{-4} Ry in the energy and forces, respectively, were used for geometry relaxation. The wavefunction and density planewave expansion cutoffs were set to 80 and 800 Ry, respectively. The initial relaxation of the quartz surface used a $2 \times 2 \times 1$ k-point mesh, while all calculations involving free or adsorbed amino acids used only the Γ point. The PAW pseudopotentials for B86bPBE were generated from datasets included in the Quantum ESPRESSO package using the `ld1.x` program.

3 Results and Discussion

3.1 Hydrogen-Bonding: Glycine and Serine

The first amino acid considered is glycine, which is not chiral. The glycine binding motifs serve as a template for adsorption of the other amino acids. As seen by Han and Sholl,[34] there are two competing low-energy configurations for glycine adsorption on the quartz surface, shown in Figure 3(a,b). Each exhibits a "staple" motif, involving two strong OH–O hydrogen bonds between the carboxylic acid group and the surface, as well as one strong OH–N hydrogen bond from the surface to the amine lone pair, shown in green in Figure 3(a,b). The NH–O distances (2.08 Å in the "A" configuration and 2.33 Å in the "B" configuration) are significantly longer than the OH–O or OH–N distances, and are not shown as hydrogen bonds in the figure.

While Han and Sholl[34] predicted the two adsorbed configurations of glycine to be effectively degenerate, we instead find that the "B" structure is more stable, by 1.8 kcal/mol. The origin of this energy difference stems from more favourable H-bonding in the B configuration. This is most evident from the differences in the COOH–OH hydrogen-bonding arrangement, where the carboxylic acid donates a H-bond to the lone pair of one the surface OH groups. In the B configuration, the dipoles of both OH groups are aligned, with an OH–OH dihedral angle of 179°; this can be contrasted with the A configuration, where the dipoles are opposing, with an OH–OH dihedral of 3°. Additionally, this COOH–OH hydrogen-bond distance is significantly shorter in the B configuration (viz. 1.70 Å versus 1.82 Å for A). It is therefore likely that the differences between the present results and those of Han and Sholl[34] for glycine are not due to the inclusion of a dispersion correction, but rather come from using a different base density functional to describe H-bonding. As noted above, this previous study employed PW91, which is known to overestimate H-bonding strengths, and also mimics short-range dispersion binding in some cases due to spurious behaviour of the exchange functional.[37–39] Also, the present work employs the projector augmented-wave approach, while Han and Sholl used ultrasoft pseudopotentials.

For the most-stable B configuration of glycine, the total adsorption energy is 25.3 kcal/mol, of which 16.6 kcal/mol is due to the base density functional. This is consistent with two OH–O hydrogen bonds ($\sim$5 kcal/mol each in water dimer[60]) and one OH–N hydrogen bond ($\sim$6.5 kcal/mol for water and ammonia[60]) between the glycine molecule and the surface. Dispersion interactions are responsible for the remaining 8.7 kcal/mol, or roughly one third of the total adsorption energy, highlighting their importance in surface adsorption studies, even in cases with strong surface-substrate hydrogen bonding.

Next we consider serine; the minimum-energy structures for adsorption of the S and R enantiomers on the quartz surface are shown in Figure 3(c,d). Here, the staple-like hydrogen-bonding motifs involving the COOH groups for the S and R enantiomers are comparable to those seen in the glycine-A and -B configurations, respectively. However, the minimum-energy structures involve H-bonding to the hydroxyl group of the side chain, rather than the amine moiety, as it is able to act as both a H-bond donor and acceptor to OH groups on the quartz surface. The NH_2 group is consequently farther from the surface and the NH–O distances (2.54 and 2.78 Å for S and R, respectively) are too long for hydrogen bonding.

As shown in Table 1, the overall adsorption energies are weaker than for glycine, despite the greater number of H-bonds between the adsorbed amino acid and the surface. This is due to the presence of a stabilizing intramolecular H-bond, from the side-chain OH to the amine lone pair, that is present in the isolated amino acid, but absent in the adsorbed configuration. The dispersion contributions to the adsorption energies are similar to glycine and effectively identical for both R and S enantiomers. In contrast to the glycine-A and -B configurations, the minimum-energy structures for the R and S enantiomers of serine are predicted to be effectively degenerate. While the COOH–OH hydrogen-bonds remain shorter and stronger for the R enantiomer than for the S (viz. 1.72 Å vs. 1.82 Å), this is offset by more a more favourable intramolecular conformation for the S enantiomer on the surface. For the S form there is a stabilizing interaction between

Fig. 3 Low-energy arrangements of glycine and serine on the hydroxylated quartz surface. Yellow lines indicate hydrogen-bonding between surface atoms, while green lines indicate hydrogen-bonding between the adsorbed amino acid and the surface. The computed adsorption energies, in kcal/mol, and the dispersion contributions (in parentheses) are also shown.

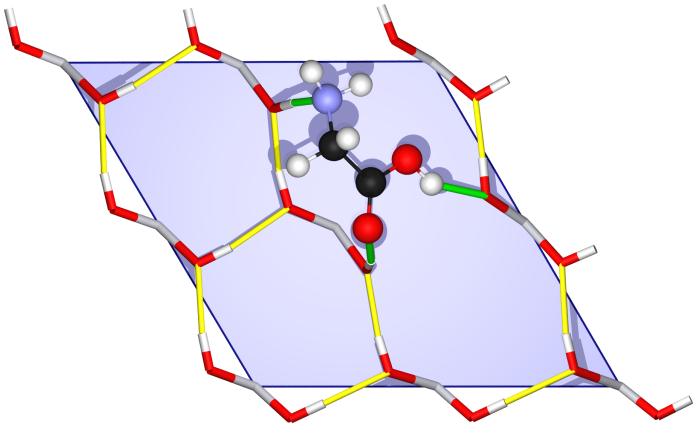

(a) Glycine A: 23.5 (9.1) kcal/mol

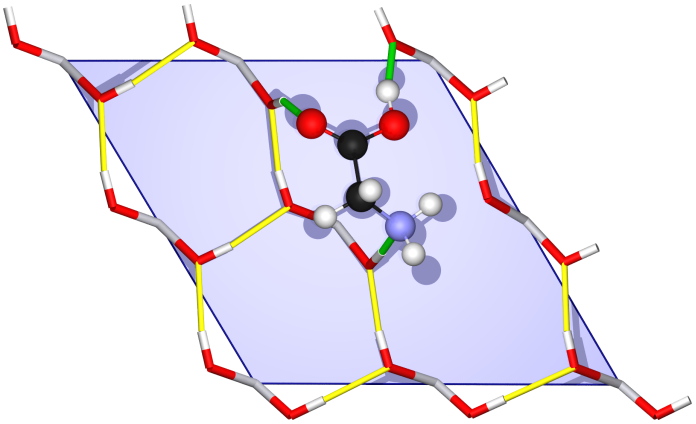

(b) Glycine B: 25.3 (8.7) kcal/mol

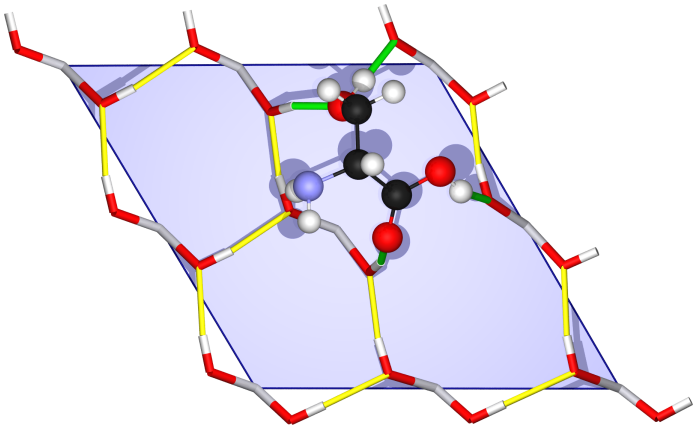

(c) Serine S: 24.2 (9.4) kcal/mol

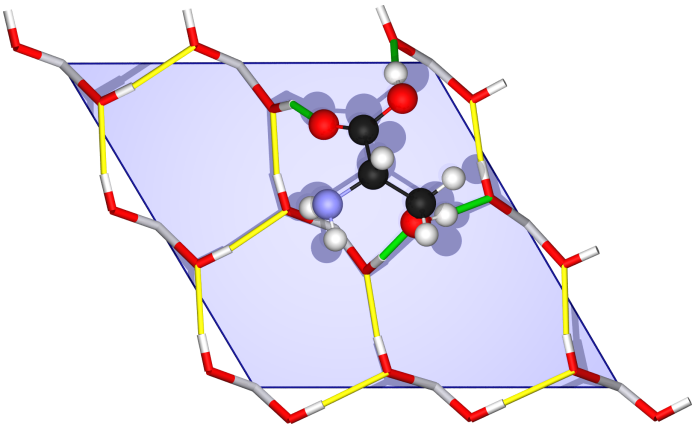

(d) Serine R: 24.3 (9.3) kcal/mol

Table 1 Computed B86bPBE-XDM adsorption energies, in kcal/mol, for selected amino acids on the hydroxylated α-quartz surface. E_{tot} refers to the total adsorption energies and E_{disp} to the XDM dispersion contributions. The difference in total adsorption energies between the most stable configurations for the R and S enantiomers, Δ, is also reported. The values for Gly are shown for comparison, although it is not chiral.

Amino acid	S		R		Δ	
	E_{tot}	E_{disp}	E_{tot}	E_{disp}	Δ_{tot}	Δ_{disp}
Gly	25.3	8.7	25.3	8.7	–	–
Ser	24.2	9.4	24.3	9.3	0.1	-0.1
Ala	25.6	9.0	26.6	10.2	1.0	1.2
Val	26.7	10.4	26.5	11.2	-0.2	0.8
Phe	27.5	14.7 10.5	29.3	14.3	1.8	-0.4 3.8

the NH bond and the carbonyl lone pairs, while for R form there is a destabilizing interaction between the adjacent N and O lone pairs. The intramolecular energy difference for this conformation change is 1.7 kcal/mol, which almost exactly offsets the contribution from intermolecular H-bonding. Thus, significant variations in intermolecular H-bonding may not be sufficient to ensure enantioselectivity.

While our minimum-energy structures for serine are in agreement with the findings of Han and Sholl,[34] our predicted lack of enantioselectivity is not. Rather, that work computed a 1.2 kcal/mol adsorption-energy difference, with the S enantiomer being more strongly bound to the surface. This difference in results emphasises that the predicted enantioselectivity is highly dependent on the choice of electronic-structure method. As with homochiral versus heterochiral crystal packings,[33,54] accurate electronic structure methods must be used to capture the many competing intermolecular interactions, including dispersion, that contribute to these subtle energy differences.

3.2 Dispersion: Alanine, Valine, and Phenylalanine

For alanine, the most-stable adsorbed structures, shown in Figure 4(a,b) for both enantiomers, are analogous to the glycine-B structure to optimise the intermolecular H-bonding. This causes the methyl group to point either toward or away from the surface for the R and S enantiomers, respectively. The adsorption energies are incrementally higher than that obtained for glycine, by 1.3 and 0.3 kcal/mol for the R and S enantiomers, respectively. The increased binding is entirely due to the increased dispersion

Fig. 4 Low-energy arrangements of alanine and valine on the hydroxylated quartz surface. Yellow lines indicate hydrogen-bonding between surface atoms, while green lines indicate hydrogen-bonding between the adsorbed amino acid and the surface. The computed adsorption energies, in kcal/mol, and the dispersion contributions (in parentheses) are also shown.

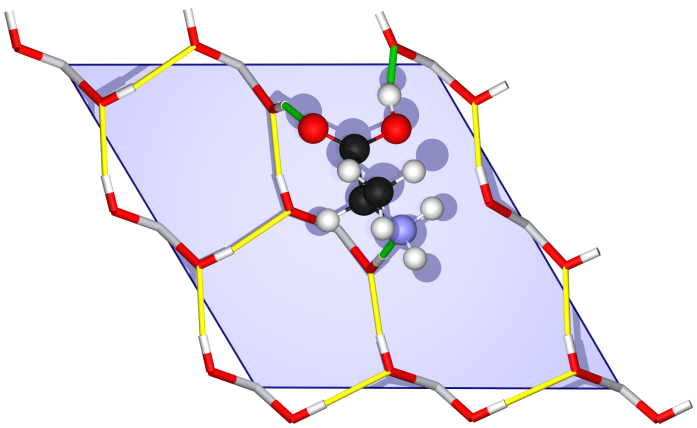

(a) Alanine S: 25.6 (9.0) kcal/mol

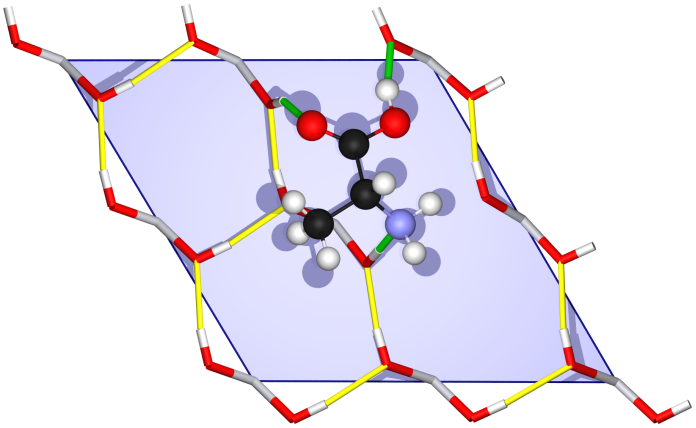

(b) Alanine R: 26.6 (10.2) kcal/mol

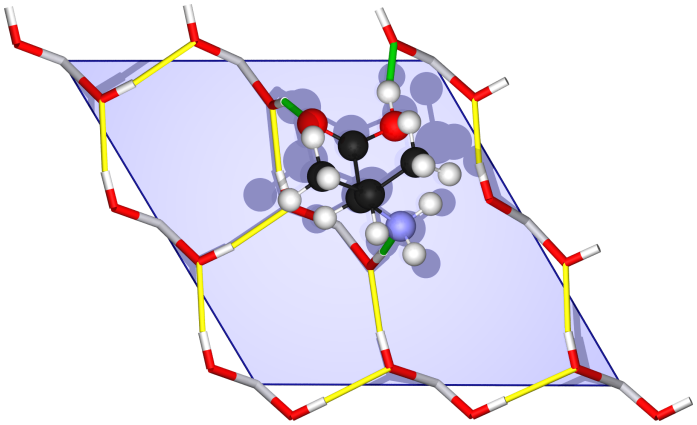

(c) Valine S: 26.7 (10.4) kcal/mol

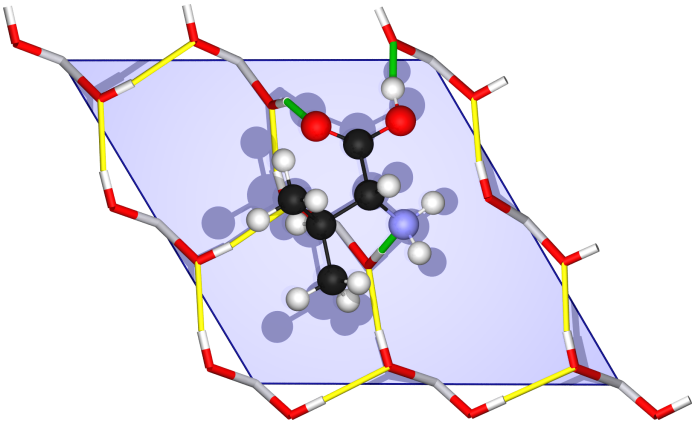

(d) Valine R: 26.5 (11.2) kcal/mol

stabilization resulting from replacement of one hydrogen atom of glycine with a methyl group in alanine. The contrasting orientations of the methyl group with respect to the surface account for the increased dispersion stabilization of the R form, which leads to the 1.0 kcal/mol difference in adsorption energy between the two enantiomers. This result agrees with our 3-point interaction model described above and demonstrates that, while being the weakest intermolecular interaction, it is possible for dispersion to control enantioselectivity.

It should be noted that an alternative adsorbed configuration for the alanine S enantiomer could be constructed[34] based on the A structure of glycine, shown in Figure 3(a). Such a geometry would have the methyl group pointing towards the surface, maximizing dispersion. However, the additional stabilization gained from dispersion (1.0 kcal/mol) is insufficient to overcome the less favourable H-bonding arrangement (1.8 kcal/mol), resulting in an adsorption energy that is 0.8 kcal/mol less than that obtained for our minimum-energy structure shown in Figure 4(a).

The alanine results imply that even greater enantioselectivity could potentially be obtained by increasing the steric bulk of the side chain, and hence its dispersion interaction with the surface. This prompted the choice of valine and phenylalanine, where the methyl side-chain is replaced by an isopropyl or phenyl substituent, respectively, for further investigation.

The minimum-energy adsorbed valine structures are shown in Figure 4(c,d) and are comparable to those obtained for alanine. The optimal intermolecular H-bonding arrangement is maintained, with the isopropyl group directed towards or away from the surface for the R and S enantiomers, respectively. For the R form, the dispersion contribution to the absorption energy is 1 kcal/mol higher than for alanine, as expected given the bulkier side-chain. However, while we expected the overall adsorption energy for the valine R enantiomer to be similarly larger than for alanine R, this is not the case. Moreover, in contrast to alanine, the adsorption energies for the R and S forms of valine are nearly equal, with a slight preference for the S enantiomer. As for serine, this can be traced to differing intramolecular interactions. The conformation adopted by the R form is 0.7 kcal/mol higher in energy than that adopted by the S form, and 1.0 kcal/mol higher than the global minimum for the isolated amino acid. Thus, our simple 3-point model breaks down for valine, due to the competition between intermolecular surface-substrate interactions and changes in intramolecular conformation.

Finally, we consider phenylalanine; the minimum-energy ar-

Fig. 5 Low-energy arrangements of phenylalanine on the hydroxylated quartz surface. Yellow lines indicate hydrogen-bonding between surface atoms, while green lines indicate hydrogen-bonding between the adsorbed amino acid and the surface. The computed adsorption energies, in kcal/mol, and the dispersion contributions (in parentheses) are also shown.

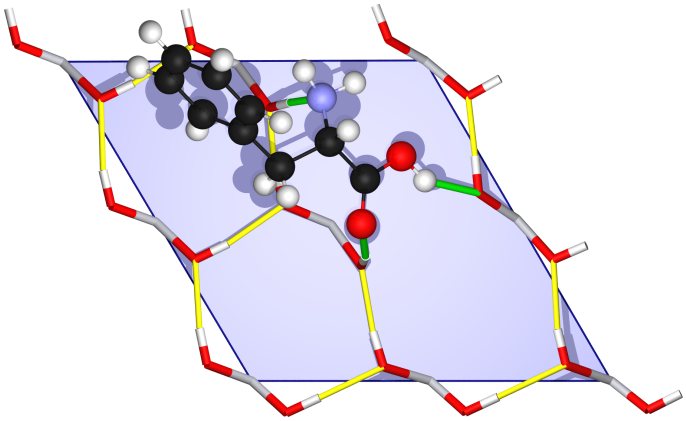

(a) Phenylalanine S_A: 27.5 (14.7) kcal/mol

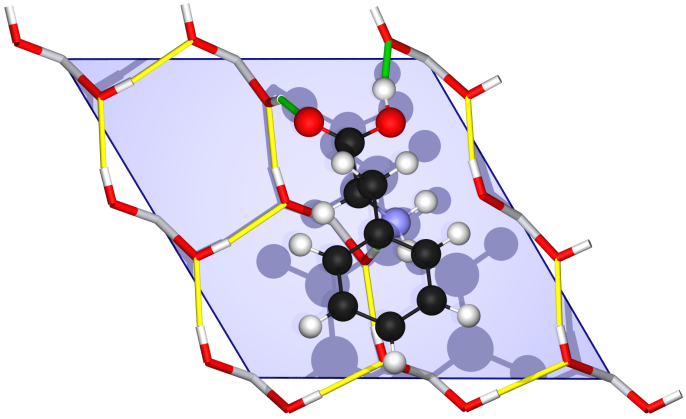

(b) Phenylalanine S_B: 27.5 (10.5) kcal/mol

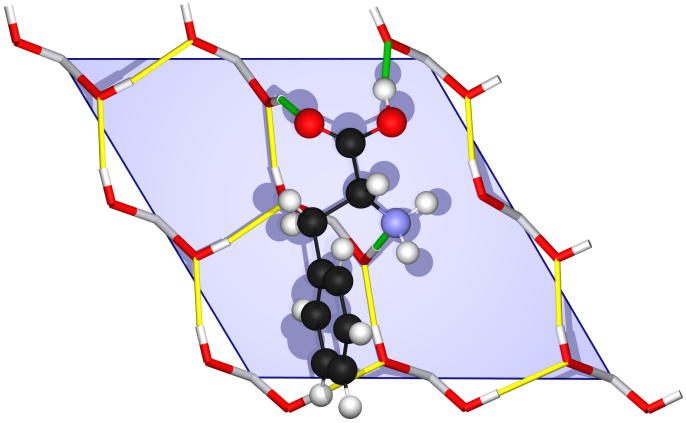

(c) Phenylalanine R: 29.3 (14.3) kcal/mol

rangements for its adsorption on the quartz surface are shown in Figure 5. The binding motif for the R enantiomer in Figure 5(c) is again analogous to that seen for alanine. The total adsorption energy and the dispersion contribution are both higher than for alanine, by 2.7 and 4.1 kcal/mol, respectively, due to favourable dispersion interactions between the phenyl ring and the surface.

For the phenylalanine S entantiomer, two low-energy configurations are possible. The configuration shown in Figure 5(b), is similar to that seen for the alanine S enantiomer. It maximises intermolecular hydrogen bonding at the expense of the phenyl ring being farther from the surface. Here, the dispersion contribution to the adsorption energy is only 1.5 kcal/mol higher than seen for the alanine S form and 0.1 kcal/mol higher than for the valine S form. The alternative, shown in Figure 5(a), is similar to the glycine-A configuration. It possesses less-favourable intermolecular H-bonding, but maximises dispersion interactions between the phenyl ring and the surface. Coincidently, these competing factors exactly offset for phenylalanine, and the two configurations for the S enantiomer are effectively degenerate. Thus, regardless of which S configuration is considered, it has an adsorption energy 1.8 kcal/mol lower than for the R enantiomer, resulting in the largest enantioselectivity seen for our set of four chiral amino acids.

Given the energetic degeneracy, there are two different ways we can interpret the enantioselectively in phenylalanine. For the S_B configuration in Figure 5(b), the enantioselectively is explained through the 3-point model, as discussed above for alanine. Here, the intermolecular H-bonding motif is conserved between the R and S forms and the enantioselectively arises from the greater dispersion binding between the phenyl ring and the surface for the R enantiomer. Conversely, for the S_A configuration in Figure 5(a), we can consider the dispersion interaction between the phenyl ring and the surface as conserved and the H-bonding arrangement switched between the R and S forms.

Phenylalanine likely provides the maximum enantioselectivity we can obtain for a family of amino acids with non-polar side chains. Increasing the steric bulk from methyl to phenyl results in increased enantioselectively. However, any further increases in steric bulk (as could be obtained with tryptophan, for example) would result in the dispersion contribution exceeding H-bonding, leading to the A configuration being consistently favoured. Hence, any further increases is steric bulk would be expected to result in a consistent 1.8 kcal/mol bias in favour of the R enantomer due to the stronger H-bonding in the B configuration.

4 Summary

In this work, we applied dispersion-corrected density-functional theory to study the adsorption of one achiral and four chiral amino acids on the (0001) face of a chiral quartz surface and to assess any enantioselectivity. The results stand in contrast with previous work[34] using the same surface face, but using a different base density functional and not employing any dispersion correction. However, dispersion interactions are shown to be responsible for 30–50% of the total adsorption energies and all of the predicted enantioselectivity for alanine. Thus, inclusion of dispersion is essential for an accurate prediction of the small differences in adsorption energies between enantiomers.

Here, the quartz surface provides considerable enantioselectivity for two of the four chiral amino acids considered, with adsorption-energy differences between the R and S enantiomers of 1.0 and 1.8 kcal/mol for alanine and phenylalanine, respectively. The alanine and phenylalanine results can be interpreted

through a simple 3-point model with the H-bonding sites conserved; the preferential binding of one enantiomer over the other thus arises from differences in dispersion interactions between the side-chain and the surface. Historically, 3-point models have focused on differences in hydrogen-bonding between enantiomers,[28,29] but this work shows that differences in London dispersion, a much weaker intermolecular interaction, can be sufficient to impart enantioselectivity.

Additionally, the greater enantioselectivity seen for phenylalanine can be explained by its greater steric bulk, relative to alanine, and hence its increased capacity for dispersion binding with the surface. Replacement of the phenyl ring with even more bulky substituents would be expected to maintain a similar level of enantioselectivity, as further increases in dispersion binding with the surface would result in a change in the H-bonding motif to maximise the adsorption energy.

Our prediction of enantioselectivity for alanine is in qualitative agreement with previous experimental findings,[24,25] although those works found only a ca. 1-2% enantiomeric enrichment. One factor inhibiting quantitative comparison is that DFT studies are limited to gas-phase simulations of neutral amino acids, rather than adsorption of zwitterionic amino acids from solution. Another is neglect of thermal free-energy corrections resulting from molecular vibrations. However, perhaps an even more important issue is that the previous experimental studies used powdered quartz. This severely limits the potential enantioselectivity by employing a mixture of many surface faces, which may have competing chiral preferences, effectively providing an ensemble average.[2] Ideally, future experimental work could be performed using a single crystallographic plane of pure left- or right-handed quartz to verify our prediction that dispersion interactions can impart enantioselectively for chiral amino-acid adsorption.

Conflicts of interest

There are no conflicts to declare.

Acknowledgements

The authors gratefully acknowledge the Natural Sciences and Engineering Research Council (NSERC) of Canada for financial support and Compute Canada for computational resources. We also thank Drs. Alex Paterson and Luc LeBlanc for helpful comments on the manuscript.

References

1 A. J. Gellman and D. S. Sholl, *AIChE*, 2009, **55**, 2484–2490.
2 R. M. Hazen and D. S. Sholl, *Nat. Mater.*, 2003, **2**, 367–374.
3 H.-S. Wang and J.-P. Wei, *Nanoscale*, 2015, **7**, 11815–11832.
4 Y. Mastai, *Chem. Soc. Rev.*, 2009, **38**, 772–780.
5 D. S. Sholl, A. Asthagiri and T. D. Power, *J. Chem. Phys.*, 2001, **105**, 4771–4782.
6 L. C. Preiss, L. Werber, V. Fischer, S. Hanif, K. Landfester, Y. Mastai and R. M. noz Espí, *Adv. Mater.*, 2015, **27**, 2728–2732.
7 T. Menahem and Y. Mastai, *J. Polym. Sci. Pol. Chem.*, 2006, **44**, 3009–3017.
8 D. D. Medina, J. Goldshtein, S. Margel and Y. Mastai, *Adv. Funct. Mater.*, 2007, **17**, 944–950.
9 J. Chen and A. S. Myerson, *CrystEngComm*, 2012, **14**, 8326–8329.
10 D. H. Dressler and Y. Mastai, *Chirality*, 2007, **19**, 358–365.
11 D. H. Dressler and Y. Mastai, *J. Colloid Interface Sci.*, 2007, **310**, 653–600.
12 J. D. Horvath and A. J. Gellman, *J. Chem. Soc.*, 2001, **123**, 7953–7954.
13 M. J. Gladys, J. W. Han, T. S. Pedersen, A. Tadich, K. M. O'Donnell and L. Thomsen, *Phys. Chem. Chem. Phys.*, 2017, **19**, 13562–13570.
14 M. J. Gladys, K. O'Donnell, A. Tadich, H. Yook, J. W. Han and L. Thomsen, *J. Phys. Chem. C*, 2019, **123**, 20829–20837.
15 Y. Yun and A. J. Gellman, *Angew. Chem. Int. Ed.*, 2013, **52**, 3394–3397.
16 Y. Huang and A. J. Gellman, *Catal. Lett.*, 2008, **125**, 177–182.
17 J. W. Han, *Top. Catal.*, 2012, **55**, 243–259.
18 K. Soai, S. Osanai, K. Kadowaki, S. Yonekubo, T. Shibata and I. Sato, *J. Am. Chem. Soc.*, 1999, **121**, 11235–11236.
19 P. R. Kavasmaneck and W. A. Bonner, *J. Am. Chem. Soc.*, 1977, **99**, 44–50.
20 T. Hitz and P. L. Luisi, *Helv. Chim. Acta*, 2002, **85**, 3975–3983.
21 D. G. Blackmond, *Cold Spring Harb. Perspect Biol.*, 2010, **2**, a002147.
22 W. A. Bonner, P. R. Kavasmaneck and F. S. Martin, *Orig. Life*, 1975, **6**, 367–376.
23 R. M. Hazen, *Am. Mineral.*, 2006, **91**, 1715–1729.
24 W. A. Bonner, P. R. Kavasmaneck and F. S. Martin, *Science*, 1974, **186**, 143–144.
25 W. A. Bonner and P. R. Kavasmaneck, *J. Org. Chem.*, 1976, **41**, 2225–2226.
26 F. Zaera, *Chem. Soc. Rev.*, 2017, **46**, 7374–7398.
27 M. Mahapatra and W. T. Tysoe, *Phys. Chem. Chem. Phys.*, 2015, **17**, 5450–5458.
28 L. H. Easson and E. Stedman, *Biochem. J.*, 1933, **27**, 1257–1266.
29 A. G. Ogston, *Nature*, 1948, **162**, 963.
30 M. S. Marshall, L. A. Burns and C. D. Sherrill, *J. Chem. Phys.*, 2011, **135**, 194102.
31 L. B. Wright and T. R. Walsh, *J. Phys. Chem. C*, 2012, **116**, 2933–2945.
32 A. Otero-de-la-Roza, J. E. Hein and E. R. Johnson, *Cryst. Growth Des.*, 2016, **16**, 6055–6059.
33 L. M. LeBlanc, A. Otero-de-la-Roza and E. R. Johnson, *J. Chem. Theory Comput.*, 2018, **14**, 2265–2276.
34 J. W. Han and D. S. Sholl, *Langmuir*, 2009, **25**, 10737–10745.
35 J. W. Han and D. S. Sholl, *Phys. Chem. Chem. Phys.*, 2010, **12**, 8024–8032.
36 J. P. Perdew, J. A. Chevary, S. H. Vosko, K. A. Jackson, M. R. Pederson, D. J. Singh and C. Fiolh ais, *Phys. Rev. B*, 1992, **46**, 6671–6687.
37 M. J. Gillan, D. Alfè and A. Michaelides, *J. Chem. Phys.*, 2016, **144**, 130901.

38 E. R. Johnson and G. A. DiLabio, *Chem. Phys. Lett.*, 2006, **419**, 333–339.
39 E. R. Johnson, R. A. Wolkow and G. A. DiLabio, *Chem. Phys. Lett.*, 2004, **394**, 334–338.
40 M. Dion, H. Rydberg, E. Schröder, D. C. Langreth and B. I. Lundqvist, *Phys. Rev. Lett.*, 2004, **92**, 246401.
41 K. Lee, É. D. Murray, L. Kong, B. I. Lundqvist and D. C. Langreth, *Phys. Rev. B*, 2010, **82**, 081101.
42 A. Dalgarno and W. D. Davison, *Adv. At. Mol. Phys.*, 1966, **2**, 1–32.
43 A. Stone, *The Theory of Intermolecular Forces*, Clarendon Press, 1997.
44 S. Grimme, J. Antony, S. Ehrlich and H. Krieg, *J. Chem. Phys.*, 2010, **132**, 154104.
45 A. D. Becke and E. R. Johnson, *J. Chem. Phys.*, 2007, **127**, 154108.
46 E. R. Johnson, in *Non-covalent Interactions in Quantum Chemistry and Physics*, ed. A. Otero-de-la-Roza and G. A. DiLabio, Elsevier, 2017, ch. 5, pp. 169–194.
47 A. Otero de la Roza and E. R. Johnson, *J. Chem. Phys.*, 2012, **136**, 174109.
48 A. Otero-de-la-Roza and E. R. Johnson, *J. Chem. Phys.*, 2013, **138**, 204109.
49 A. Otero de la Roza and E. R. Johnson, *J. Chem. Phys.*, 2012, **137**, 054103.
50 A. Otero-de-la-Roza, L. M. LeBlanc and E. R. Johnson, *J. Phys. Chem. Lett.*, 2020, **11**, 2298–2302.
51 M. S. Christian, A. Otero-De-La-Roza and E. R. Johnson, *J. Chem. Theory Comput.*, 2016, **12**, 3305.
52 M. S. Christian, A. Otero-de-la-Roza and E. R. Johnson, *Carbon*, 2017, **118**, 184–191.
53 M. S. Christian, A. Otero-de-la-Roza and E. R. Johnson, *Carbon*, 2017, **124**, 531–540.
54 A. Otero-de-la Roza, B. H. Cao, I. K. Price, J. E. Hein and E. R. Johnson, *Angew. Chem. Int. Ed.*, 2014, **53**, 7879–7882.
55 T. P. M. Goumans, A. Wander, W. A. Brown and C. R. A. Catlow, *Phys. Chem. Chem. Phys.*, 2007, **9**, 2146–2152.
56 P. Giannozzi, S. Baroni, N. Bonini, M. Calandra, R. Car, C. Cavazzoni, D. Ceresoli, G. Chiarotti, M. Cococcioni, I. Dabo, A. Dal Corso, S. Fabris, G. Fratesi, S. de Gironcoli, R. Gebauer, U. Gerstmann, C. Gougoussis, A. Kokalj, M. Lazzeri, L. Martin-Samos, N. Marzari, F. Mauri, R. Mazzarello, S. Paolini, A. Pasquarello, L. Paulatto, C. Sbraccia, S. Scandolo, G. Sclauzero, A. P. Seitsonen, A. Smogunov, P. Umari and R. M. Wentzcovitch, *J. Phys. Condens. Matter*, 2009, **21**, 395502.
57 P. E. Blöchl, *Phys. Rev. B*, 1994, **50**, 17953.
58 A. D. Becke, *J. Chem. Phys.*, 1986, **85**, 7184.
59 J. P. Perdew, K. Burke and M. Ernzerhof, *Phys. Rev. Lett.*, 1996, **77**, 3865–3868.
60 F. O. Kannemann and A. D. Becke, *J. Chem. Theory Comput.*, 2010, **6**, 1081–1088.